Transient Response of Divertor Plasma During Transition to ELM Free H-Mode Phase in JT-60U

Hidenobu TAKENAGA, Naoyuki OYAMA and Nobuyuki ASAKURA

Japan Atomic Energy Agency, Naka 311-0193, Japan

(Received 5 July 2006 / Accepted 15 August 2006)

A drop in divertor plasma density was observed during the transition to the ELM free H-mode phase as well as the drop in Dα emission intensity in JT-60U. The time scale for the drop in divertor plasma density ranged from a few ms to several tens of ms. 2-D fluid divertor code simulations indicated that the time scale for the divertor plasma density drop was ranged from several tens of ms to a hundred ms, when thermal and particle diffusivities were instantly reduced in the main plasma edge with a constant recycling coefficient. When it was assumed that the recycling coefficient decreased with a decrease in heat flux and increased with a decrease in particle flux, the time scale was reduced to a few ms in the simulations accompanied by a reduction of edge thermal diffusivity. These results indicate that the sharp drop of the divertor plasma density concomitant with the sharp drop of the Dα emission intensity on a time scale of a few ms can be ascribed to the change of plasma-wall interaction depending on the heat flux to the divertor plates.

© *2006 The Japan Society of Plasma Science and Nuclear Fusion Research*

Keywords: H-mode transition, divertor plasma density, Dα emission, divertor simulation, recycling coefficient, JT-60U

DOI: 10.1585/pfr.1.046

1. Introduction

H-mode plasma was first found in ASDEX [1] and the transition from the L-mode phase to the H-mode phase has been associated with a sharp drop of Hα or Dα emission intensity together with increases in edge density and temperature. The reduced level of the Hα/Dα emission intensity and the increases in edge density and temperature are terminated by the occurrence of edge-localized mode (ELM), after which the ELM free H-mode phase shifts to the ELMy H-mode phase with frequent spikes of Hα/Dα emission intensity. Up to now, various conditions of the H-mode phase without ELM or with small ELMs have been found. These include the enhanced Dα (EDA) H-mode in Alcator C-Mod [2], the H'-mode and the high recycling steady (HRS) H-mode in JFT-2M [3, 4], the transition-free H-mode in JT-60U [5], and the quiescent H-mode (QH-mode) in DIII-D [6]. These H-mode phases are characterized by Hα/Dα emission intensity, which is considered in relation to the particle transport at the main plasma edge. The high level of Hα/Dα emission intensity is associated with large particle flux from the main plasma due to high particle transport in the main plasma edge. Conversely, the low level of Hα/Dα emission intensity is associated with small particle flux from the main plasma due to low particle transport in the main plasma edge. However, Hα/Dα emission intensity expresses the particle flux to the divertor plates rather than the particle flux from the main plasma. The particle flux from the main plasma is much smaller than that to the divertor plates in large tokamak devices such as JT-60U, because a large fraction of the recycled neutral particles ionizes in the divertor region. Therefore, it is necessary to investigate the response of the divertor plasma against the change of the particle and heat fluxes from the main plasma in order to understand the key mechanisms determining the behavior of the Hα/Dα emission intensity observed in various conditions of the H-mode phase.

In JT-60U, the mm-wave interferometer has been developed [7] for measuring the line-integrated electron density at the upper stream of the divertor plasma, thus providing a means to investigate the transient response of the divertor plasma during the transition to the ELM free H-mode phase. In many devices, divertor plasma density and temperature are routinely measured using Langmuir probes mounted on the divertor plates. In the DIII-D lower divertor, a Thomson scattering system was installed for measuring the density and temperature at the upper stream of the divertor plasma [8]. However, the time resolution of these systems is limited by the duration of the voltage scan necessary for the probe measurement and by the laser repetition frequency of the Thomson scattering system. On the other hand, the mm-wave interferometer can measure the fast response of divertor plasma density, although this device has difficulty in covering the entire divertor region. For interpreting the measured results as physical mechanisms governing the phenomena in the wide divertor region, comparison with numerical simulation results is effective. A 2-D fluid divertor code has been developed for understanding the heat and particle transport characteris-

author's e-mail: takenaga.hidenobu@jaea.go.jp

© 2006 The Japan Society of Plasma Science and Nuclear Fusion Research

tics of the divertor and SOL plasmas [9–11]. A comparison between calculations and measurements has been performed in the steady-state phase [12]. Recently, transient analysis has been emphasized in relation to the transient heat load induced by an ELM [13], thus increasing the capabilities of the time-dependent simulations.

In this paper, divertor plasma density was measured together with Dα emission intensity and the particle flux to the divertor plates during the transition to the ELM free H-mode phase. The measured results were compared with time-dependent simulations using the 2-D fluid divertor code UEDGE [10] for understanding the transient response of the divertor plasma. In Sec. 2, the diagnostic arrangements related to this study are described. The measured results are discussed in Sec. 3. In Sec. 4, the measured results are compared with the time-dependent simulations. In Sec. 5, a discussion is presented based on the results obtained in the previous sections, followed by a summary in Sec. 6.

2. Diagnostic Arrangements

In JT-60U, a W-shaped divertor has been installed with the divertor pumping from both the inner and outer private flux regions [14]. The typical divertor configuration is shown in Fig. 1 together with the sight lines and positions of the diagnostics related to this study. The inner and outer inclined divertor plates and the divertor dome in the private flux region form a W-shaped surface connected to the inner and outer baffle plates. Carbon-fiber composite (CFC) tiles are used for the divertor plates, the divertor dome top, and the outer wing of the divertor dome, while graphite tiles are used for the divertor dome's inner wing and the baffle plates. Toroidally continuous pumping slots are arranged between the divertor plates and the divertor dome wings. The width of the pumping slot is set at 3 cm for the inner divertor and 2 cm for the outer divertor, respectively.

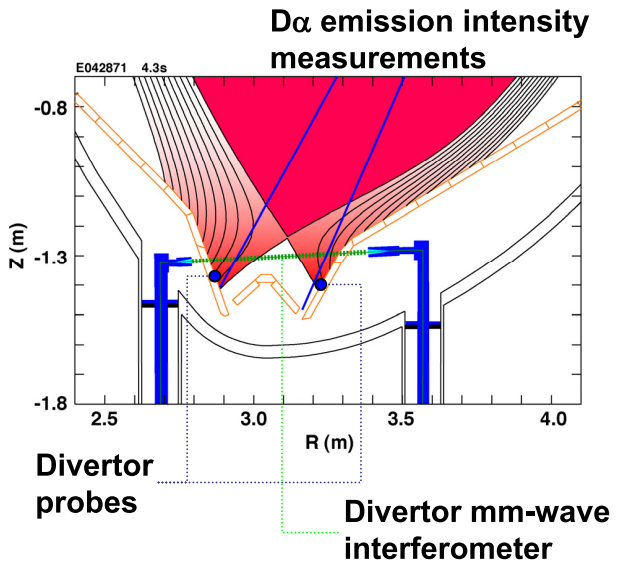

Fig. 1 Schematic drawing of typical divertor configuration and diagnostic arrangements related to this study.

The line-integrated electron density at the upper stream of the divertor region was measured using a mm-wave interferometer [7]. The wave-guide system installed in the divertor region allows flexible access to the complicated divertor geometry, as shown in Fig. 1. The sight line passes horizontally below the X-point. A transmitter and receiver unit with a frequency of 183 GHz was employed, with a cut-off density of $4.1 \times 10^{20}\,\mathrm{m}^{-3}$. The data was recorded at a sampling time of 5 - 10 μs. The Dα emission intensities were measured using a fiber array whose detectors were absolutely calibrated using an integrating sphere. In the present study, measuring chords covering the inner and outer divertor regions as shown in Fig. 1 were used. The data was recorded at a sampling time of 5 - 40 μs. The Dα emission intensity signal from the outer divertor was synchronized with the divertor plasma density signal using the same data acquisition system. Langmuir probes placed on the divertor plates near the strike points were used for the measurement of the particle flux to the divertor plates with a high constant voltage of −150 V. The data was recorded at a sampling time of 40 μs. The line-averaged electron density in the main plasma was measured using far infrared interferometers with two measuring chords utilizing the vertical ports similar to the ports for the mm-wave interferometer.

3. Time evolution of the Divertor Plasma during Transition to ELM Free H-Mode

Figure 2 shows the waveforms during the transition to the ELM free H-mode with a plasma current of I_p = 1.0 MA and a toroidal magnetic field of B_T = 2.7 T. A constant neutral beam (NB) heating power of P_{NB} = 12 MW was applied from t = 4.05 s, although NB breakdown occurred during t = 4.15 - 4.2 s. In this discharge, the complex features of the transition phenomena were observed. It seems that there were three phases before the ELMy H-mode phase, these being the L-mode phase and two different phases of the H-mode as shown by the symbols of L, H_1, and H_2 at upper part of Fig. 2. Here, the phase with a small reduction of edge transport was categorized as the H_1-mode, and the phase with a large reduction of the edge transport was categorized as the H_2-mode.

The first transition from the L- to the H_1-mode phase at t = 4.15 s is not clearly observed in the edge electron temperature at r/a = 0.9 and the edge line-averaged electron density, probably due to the effect of NB breakdown and the small reduction of the edge transport. However, the Dα emission intensity and the divertor plasma density began to decrease gradually even with the increase in the

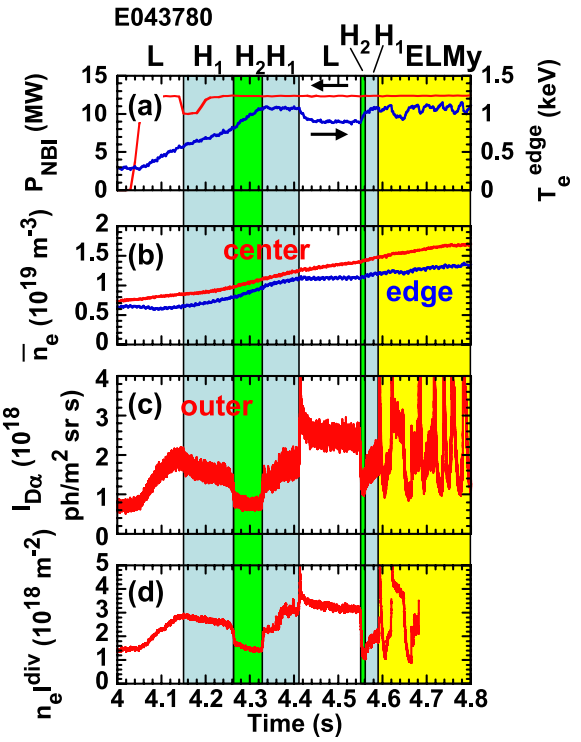

Fig. 2 Time behavior of (a) NB heating power and edge electron temperature at $r/a = 0.9$, (b) center and edge line-averaged electron density, (c) Dα emission intensity from the outer divertor, and (d) line-integrated divertor electron density. The characters shown in the upper part of the figure indicate the plasma confinement phase.

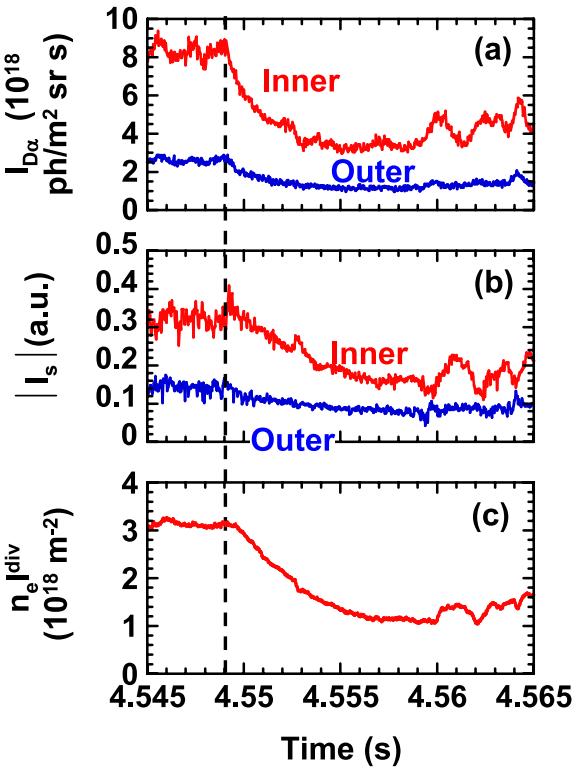

Fig. 3 Expanded view of (a) Dα emission intensities from the inner divertor (red line) and outer divertor (blue line), (b) absolute value of ion saturation current for the inner divertor (red line) and the outer divertor (blue line), and (c) line-integrated electron density during the transition from the L- to the H_2-phase ($t = 4.545$ - 4.565 s) in the discharge shown in Fig. 2.

electron density in the main plasma during the H_1-mode phase. These signals indicate the occurrence of the phase transition to the H-mode. The transition from the H_1- to the H_2-mode phase was induced with a sharp drop of the Dα emission intensity at $t = 4.26$ s due to further reduction of the edge transport. The edge electron temperature at $r/a = 0.9$ around the pedestal top and the edge line-averaged electron density largely increased during the H_2-mode phase. It can be seen from this figure that the divertor plasma density abruptly dropped being concomitant with the Dα emission intensity during the transition. The increase in the edge electron temperature was terminated by the back transition from the H_2- to the H_1-mode phase at $t = 4.33$ s due to enhanced edge transport. The edge line-averaged electron density continued to increase at a smaller rate during the H_1-mode phase. The Dα emission intensity and the divertor plasma density increased to the same levels as those before the H_1-H_2 transition.

After the back transition from the H_1- to the L-mode phase triggered by the ELM, the edge electron temperature decreased and the increase in the edge line-averaged electron density was terminated. The levels of the Dα emission intensity and the divertor plasma density were larger than those in the H_1 and H_2-mode phases. It is noted that the divertor plasma density cannot be measured during the back transition to the L-mode phase when the signal intensity was reduced significantly. Therefore, the integer part of the interferometer fringe after the back transition was adjusted to that before the transition. Refraction can be considered a candidate for the physical procedure for reducing the signal.

The transition from the L- to the H_2-mode phase and the back transition from the H_2- to the H_1-mode phase were induced at $t = 4.55$ s and 4.56 s, respectively. The ELMy H-mode phase was then initiated. A sharp drop of the divertor plasma density was also observed as well as a sharp drop of the Dα emission intensity at the transition from the L- to the H_2-mode phase. The central density continued to increase in all phases, but the increase rate was the largest in the H_2-mode phase. These observations indicate the existence of multiple levels of transport reduction in the H-mode plasma similar to that of the EDA H-mode, the H'-mode, and the HRS H-mode. This paper focuses on the sharp drop in the divertor plasma density observed at the transitions to the H_2-mode phase concomitant with the drop of the Dα emission intensity.

Figure 3 shows an expanded view of the divertor plasma density during the transition from the L- to the

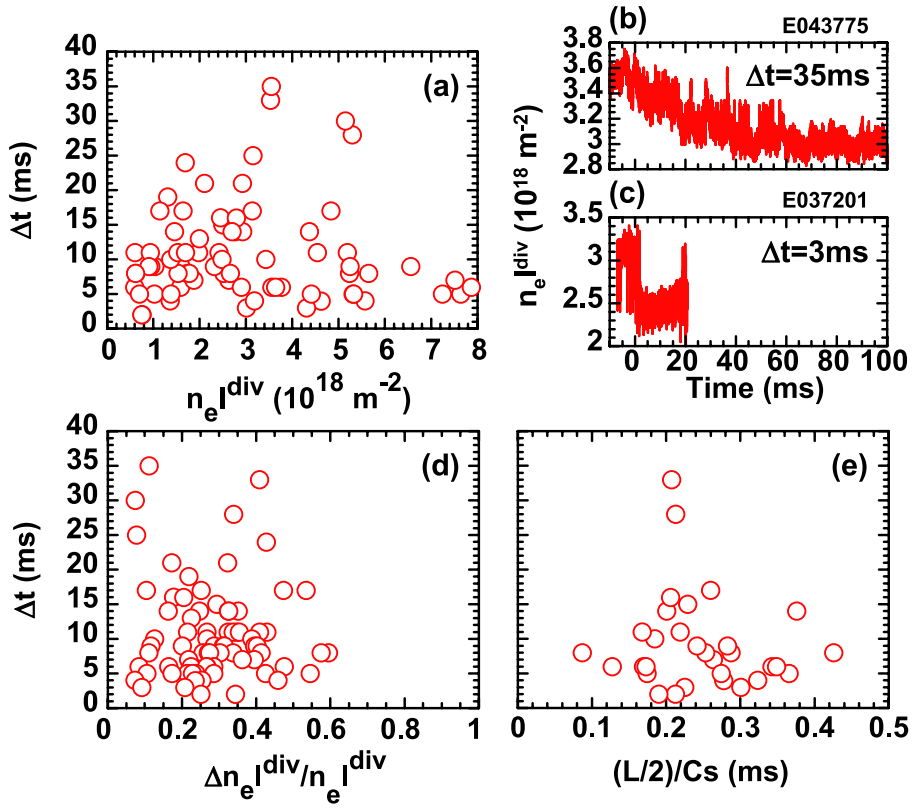

Fig. 4 (a) Time scale of the drop in divertor plasma density as a function of line-integrated divertor plasma density before the transition. Typical waveform of the divertor plasma density for (b) the longer time scale case and (c) the shorter time scale case. Time scale of the drop in divertor plasma density as a function of (d) reduction ratio and (e) the time scale of particle flow from the main plasma to the divertor plasma.

H_2-mode phase (t = 4.545 - 4.565 s) together with the Dα emission intensities and the absolute value of the ion saturation currents measured with the Langmuir probes. The Dα emission intensities from the inner and outer divertor regions were simultaneously reduced as shown in Fig. 3 (a). The ion saturation current was also reduced at the same time for the outer divertor region. The ion saturation current for the inner divertor region seems to slightly increase at the immediate start of the reduction of Dα emission intensity. This increase might be related to the reduction of non-thermal electron flux to the divertor plate due to the improvement of the non-thermal electron transport in relation to the change of the edge electric field during the transition. The divertor plasma density began to decrease at ~0.5 ms after the reduction of the Dα emission intensities on a time scale of ~8 ms. Such a delay in the reduction of divertor plasma density was observed in many cases which have a relatively short time scale of several ms for the reduction of divertor plasma density. This delay was also observed at the transition from the H_1 to the H_2-mode phase. The delayed reduction of divertor plasma density indicates that the reduction of the heat and particle fluxes escaping from the main plasma decreases the divertor plasma density through the change of the recycling and/or the divertor plasma parameters, but it does not decrease the divertor plasma density directly.

The time scale of the drop in divertor plasma density could be related to the time scale of the change in divertor plasma. Therefore, the dependence of the time scale for reduction of divertor plasma density on the divertor plasma parameters was investigated. Figure 4 (a) shows the time scale of the drop in divertor plasma density as a function of the line-integrated divertor plasma density before the transition. The database was accumulated with I_p = 0.4 - 2 MA, B_T = 1.7 - 4 T, $\bar{n}_e$ = 1.7 - 2.4 × 10^{19} m^{-3}, and P_{NB} = 1 - 20 MW. The time scale was varied in the range of a few ms to several tens of ms. Two typical waveforms are shown in Fig. 4 (b) in the case of a large time scale (gradual drop) and (c) for the case of a small time scale (sharp drop). No clear dependence of the time scale on the line-integrated divertor plasma density was observed. The time scale of the divertor plasma density drop also showed no dependence on its reduction ratio, as shown in Fig. 4 (d). The time scale of the divertor plasma density drop was next compared with the time scale of the particle flow from the main plasma to the divertor plasma estimated as $(L/2)/Cs$, where L is the connection length at 1 cm outside the separatrix on the outer mid-plane and Cs is the ion sound velocity at the main plasma edge. The time scale of the divertor plasma density drop was larger than that

of the particle flow from the main plasma to the divertor plasma, with no correlation between these time scales being observed. These results suggest that the time scale of the divertor plasma density drop is determined by the time scale of the transient response of divertor plasma rather than the reduction of the particle and heat fluxes from the main plasma.

4. Simulations using 2-D Fluid Divertor Code

4.1 Simulation model

In order to investigate the mechanisms governing the time scale of the reduction of divertor plasma density, time-dependent simulations were performed using the 2-D fluid divertor code UEDGE [10]. In the UEDGE calculation, particle and power fluxes at the core boundary (80% of the poloidal magnetic flux) were set as constant boundary conditions (1×10^{21} particles/s and 5.4 MW) based on experimental results. Spatially constant anomalous diffusion coefficients were taken for electron and ion thermal diffusivities (χ_e and $\chi_i = 1\,m^2/s$) and particle diffusivity ($D = 0.25\,m^2/s$) before the transition ($t < 0$ s). These were reduced instantly at $t = 0$ s at the edge region of the main plasma (96.5 - 100% of the poloidal magnetic flux) for simulating the transition to the ELM free H-mode phase. The time evolution of the divertor plasma was then calculated. All χ_e, χ_i and D were reduced in case A. In case B, χ_e and χ_i were reduced, while only D was reduced in case C. The carbon yield rate was enhanced from the Haasz yield [15] for both physical and chemical sputtering to reproduce the divertor radiation power. The recycling coefficient at the divertor plates was set at 0.995 before the transition. After the transition, the recycling coefficient was maintained at a constant value for the former case (case A/B/C-1) and was assumed to decrease with decreasing heat flux (Q) and increase with decreasing particle flux (Φ) for the latter case (case A/B/C-2).

In the latter case, the recycling coefficient (R) was assumed as $R = C_Q(Q/Q^0 - 1) + C_\Phi(\Phi^0/\Phi - 1) + 0.995$ (C_Q, $C_\Phi > 0$). Here, C_Q and C_Φ are the constant coefficients. The recycling coefficient is determined by the balance among reflection, trapping (potential and chemical), thermal desorption, and sputtering (physical and chemical). This balance is affected by the heat and particle fluxes. The heat load could be related to the physical sputtering and/or thermal desorption. In JT-60U, the increase of the heat load introduced by the electron cyclotron heating enhanced the recycling, and the increase in the electron density was observed even without particle fuelling [16]. Enhancement of the recycling due to the transient ELM heat load was also observed in JT-60U [17]. Conversely, the reduction of the heat load could suppress the sputtering and/or the thermal desorption, resulting in a decrease in the recycling coefficient. The reduction of the particle flux could cause a decrease in trapping. When particle retention decreases, the recycling coefficient could transiently increase. Dynamic retention has been observed in JT-60U long pulse discharges [18], in which the particle retention in the first wall and the divertor plates is considered to depend on the particle and heat fluxes. Based on this idea, the recycling coefficient in the simulation was assumed to depend on the particle and heat fluxes. The wall temperature and the hydrogen retention as well as the heat and particle fluxes could also influence the balance. These effects were included in the dependence of the recycling coefficient on the heat and particle fluxes.

The comparison between the SOL flow measurements and the UEDGE calculation in JT-60U indicated the important role of the drift effects in reproducing the measured particle flow [19]. However, in order to improve the convergence of the calculation, the drift effects were not considered in this paper.

4.2 Simulation results

Figure 5 shows the time evolution of the line-integrated divertor plasma density, the Dα emission intensities from both the inner (red lines) and outer (blue lines) divertor regions, and the particle and heat fluxes to the inner (red lines) and outer (blue lines) divertor plates for the cases A/B/C-1. The line-integrated divertor plasma density and the Dα emission intensities were evaluated in the context of the diagnostic conditions. When χ_e, χ_i, and D were reduced by a factor of 10 at $t = 0$ s (case A-1: solid lines), the divertor plasma density began to decrease from $t = 0.1$ ms and had two minimum values around $t = 1$ ms and 100 ms. In this case, χ_i was reduced to the neoclassical transport level. On the other hand, there was only one minimum value around $t = 0.5$ ms in the case with a reduction of χ_e and χ_i (case B-1: dotted lines) and around $t = 100$ ms in the case with a reduction of D (case C-1: dashed lines). The reductions of the Dα emission intensity and the particle flux to the divertor plates were larger in the inner divertor than in the outer divertor, although the heat flux to the divertor plates was largely reduced in both the inner and outer divertor regions. The reduction was initiated in sequence, starting with the heat flux, then proceeding to the particle flux, the Dα emission intensity, and then the divertor plasma density. The heat flux to the divertor plates was first reduced due to higher parallel heat transport compared with parallel particle transport. The delayed reduction of the divertor plasma density from the Dα emission intensity was consistent with the measurement. The time scale of the first minimum value for case A-1 was similar to the time scale of the minimum value for case B-1, while the time scale of the second minimum value for case A-1 was similar to the time scale of the minimum value for case C-1. Therefore, the first reduction of divertor plasma density was ascribed to the reduction of the heat flux from the main plasma, while the second reduction was ascribed to the reduction of the particle flux from the main plasma.

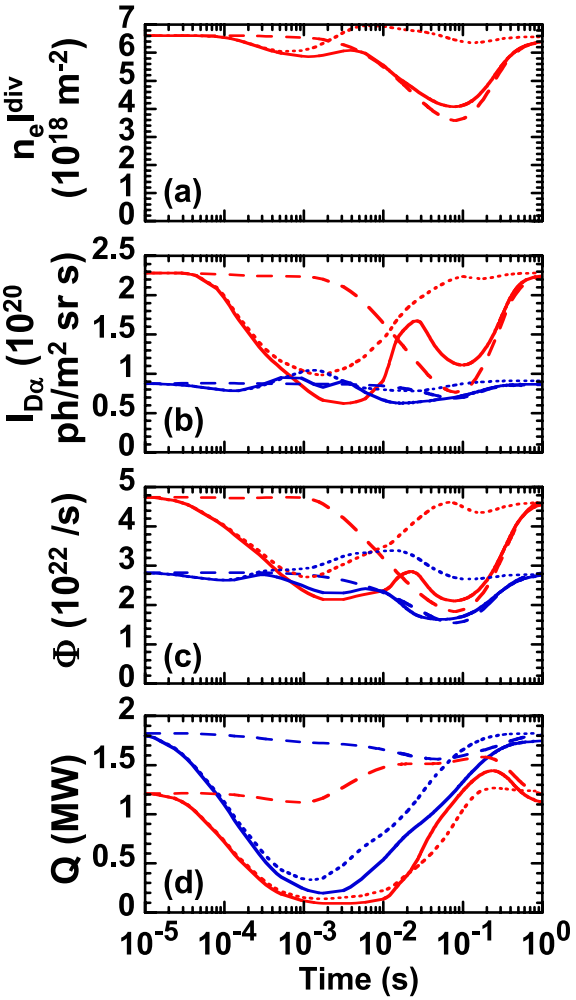

Fig. 5 Simulation results with a constant recycling coefficient. (a) Line-integrated divertor electron density, (b) Dα emission intensities from the inner divertor (red lines) and the outer divertor (blue lines), (c) particle fluxes and (d) heat fluxes to the inner divertor plates (red lines) and to the outer divertor plates (blue lines). Solid lines show the data for the case with the reduction of χ_e, χ_i, and D (case A-1). Dotted lines show the data for the case of the reduction of χ_e and χ_i (case B-1). Dashed lines show the data for the case of the reduction of D (case C-1).

The short time scale of the divertor plasma density drop with the small reduction ratio shown in Fig. 4 (d) can be explained by the reduction of the heat flux from the main plasma (case B-1). However, since the reduction ratio was small even with reductions of χ_e and χ_i to the ion neoclassical transport level, the large reduction ratio cannot be explained only by the reduction of the heat flux from the main plasma. The reduction of the particle flux from the main plasma is necessary for reproducing the large reduction ratio in these cases.

Figure 6 shows the reduction ratio of the divertor plasma density and the time scale of the reduction of divertor plasma density as a function of the ratio of χ_e, χ_i, and D after and before the transition. In these simulations,

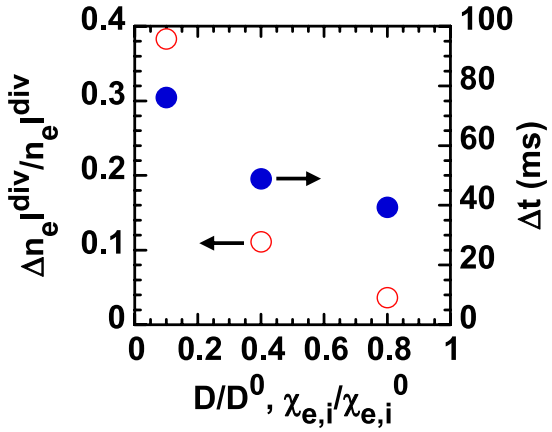

Fig. 6 Reduction ratio of the divertor plasma density (open circles) and time scale for divertor plasma density reduction (closed circles) as a function of the ratio of thermal diffusivity and particle diffusivity after and before the transition.

χ_e/χ_e^0, χ_i/χ_i^0, and D/D^0 were all set at the same value and the recycling coefficient was assumed to be constant. The data are plotted as values for the second minimum values. The reduction ratio of the divertor plasma density decreased with increasing χ_e/χ_e^0, χ_i/χ_i^0, and D/D^0. The time scale was shorter for larger χ_e/χ_e^0, χ_i/χ_i^0, and D/D^0. These simulations can explain the case of only the larger time scale with the small reduction ratio of divertor plasma density shown in Fig. 4 (d). The simulation incorporating a constant recycling coefficient can explain only the small reduction ratio with the short time scale due to the reduction of the heat flux from the main plasma and with the long time scale due to the reduction of the particle flux from the main plasma, respectively.

In order to reproduce the large reduction ratio of the divertor plasma density, the change of the plasma-wall interaction was introduced into the simulation as described in Sec. 4.1. Figure 7 shows the simulation results from $t = 10^{-5}$ to $t = 10^{-2}$ s, since numerical instability occurred after $t = 10^{-2}$ s. Here, C_Q and C_Φ were set at 0.5 and 0.2, respectively. The time scale of the divertor plasma density's reduction was evaluated to be 3 ms in the case of reductions of χ_e, χ_i, and D by a factor of 10 (case A-2: solid lines). The reduction was also performed sequentially, starting with the heat flux, then proceeding to the particle flux, the Dα emission intensity, and then to the divertor plasma density. The delayed reduction of the divertor plasma density from the Dα emission intensity was also consistent with the measurement. The recycling coefficient was reduced to ~0.7 and the divertor plasma density had a single minimum value. A short time scale was also obtained in the case with reductions of χ_e and χ_i (case B-2: dotted lines). However, divertor plasma density was not significantly reduced in the case with the reduction of only D (case C-2: dashed lines), because the recycling coeffi-

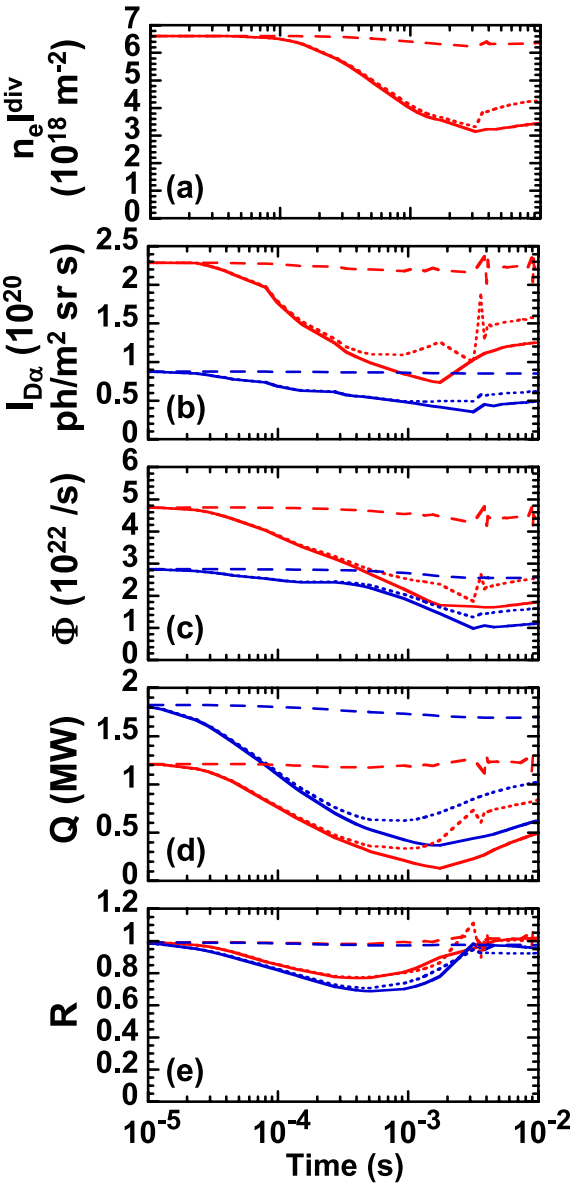

Fig. 7 The simulation results with a change of the recycling coefficient. (a) Line-integrated divertor electron density, (b) Dα emission intensities from the inner divertor (red lines) and the outer divertor (blue lines), (c) particle fluxes, and (d) heat fluxes to the inner divertor plates (red lines) and to the outer divertor plates (blue lines). Solid lines show the data for the case of the reduction of χ_e, χ_i, and D (case A-2). Dotted lines show the data for the case of the reduction of χ_e and χ_i (case B-2). Dashed lines show the data for the case of the reduction of D (case C-2).

cient increased with the decrease in particle flux. This result indicates that the sharp drop in divertor plasma density with the large reduction ratio can be ascribed to the change of plasma-wall interaction due mainly to the reduction of the heat flux from the main plasma.

Figure 8 shows the divertor densities simulated with various combinations of C_Q and C_Φ in an investigation of the sensitivity of the simulation results against the values

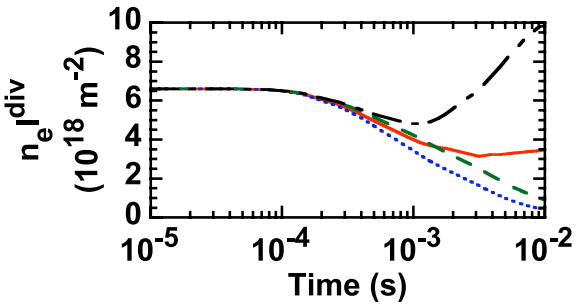

Fig. 8 Line-integrated divertor densities simulated with various C_Q and C_Φ (dashed line: $C_Q = 0.3$ and $C_\Phi = 0$, dotted line: $C_Q = 0.5$ and $C_\Phi = 0$, solid line: $C_Q = 0.5$ and $C_\Phi = 0.2$ same as the simulation shown in Fig. 7, and dash-dot-line: $C_Q = 0.5$ and $C_\Phi = 0.5$).

of C_Q and C_Φ. Here, χ_e, χ_i, and D were reduced by a factor of 10 as were those in case A. In the case of $C_\Phi = 0$, the divertor plasma density decreased greatly for both $C_Q = 0.5$ and 0.3. In the case of $C_Q = 0.5$ and $C_\Phi = 0.5$, the divertor plasma density decreased once, but increased after $t = 10^{-3}$ s and exceeded the initial value. Although unique solutions for the values of C_Q and C_Φ cannot be obtained, the combination of $C_Q = 0.5$ and $C_\Phi = 0.2$ gave reasonable results. The dependence of the recycling coefficient on the heat and particle fluxes could be affected by the wall condition. Therefore, the time scale of the divertor plasma density reduction could be affected by the wall condition. The recycling process has been investigated in detail by numerical simulations [20]. Recently, numerical simulations were developed that take into consideration molecular dynamics including those of hydrocarbons [21]. However, a systematic understanding has not yet been obtained regarding the relationship between the results of numerical simulations and the experimental results, especially in the transient phase. A detailed comparison of these numerical simulations and the experiments should be performed in the future in order to identify the mechanisms responsible for the recycling coefficient's dependence on the heat and particle fluxes.

5. Discussion

According to the above results, the divertor plasma density could drop when the heat flux to the divertor plates decreases. Such a drop has been observed for pellet injection and impurity injection during lower hybrid radio frequency (LHRF) wave heating. Figure 9 shows the time evolution of the line-integrated divertor plasma density, the line-averaged density in the main plasma edge, and the Dα emission intensity when a small pellet (2.1 mm cubic) was injected from the high-field-side at the top into the ohmic heated plasma at a slow injection speed of 120 m/s [22]. A peak in the divertor plasma density was initially observed, which could be related to pellet ablation in the SOL

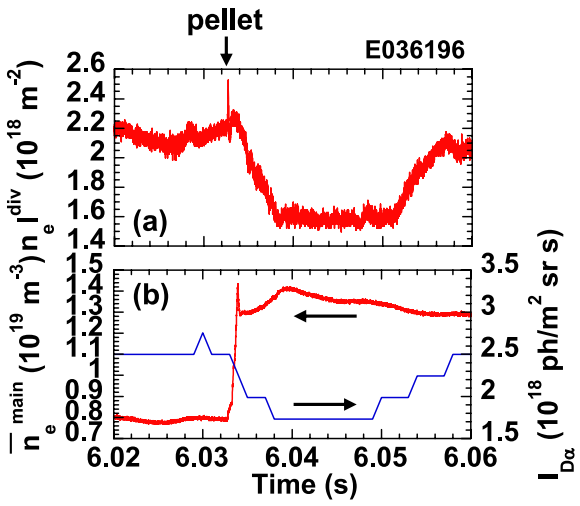

Fig. 9 (a) Divertor plasma density and (b) line-averaged edge density and Dα emission intensity from the outer divertor with small pellet injection from the high-field-side at the top.

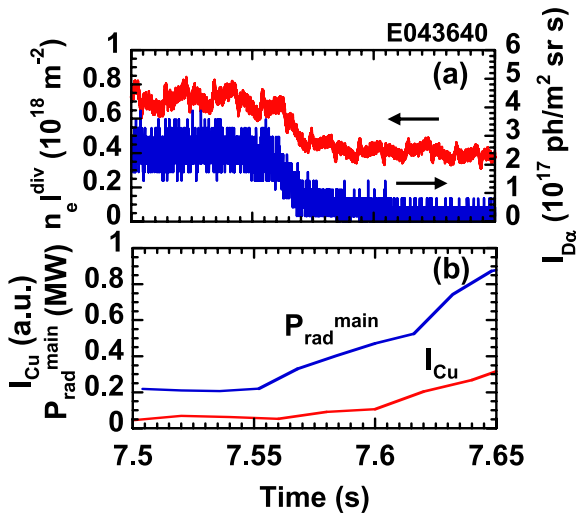

Fig. 10 (a) Divertor plasma density and Dα emission intensity and (b) Cu line and radiation loss from the main plasma in the discharge with metal impurity contamination from the LHRF wave antenna.

plasma, and the edge density then started to increase and the divertor plasma density decreased at a time scale of ~5 ms. The divertor plasma density decreased even with particle fuelling into the main plasma. The line integrated divertor plasma density was maintained at a low level for ~14 ms. The divertor Dα emission intensity also decreased just after the pellet injection. In this case, the pellet was ablated at the plasma edge; therefore, the power flux to the divertor plates could be reduced. The reduction of divertor plasma density was not observed in the case of deep penetration with low-field-side pellet injection at an injection speed of about 700 m/s.

A fast decrease in divertor plasma density was also observed when the impurity was injected from the LHRF wave antenna during LHRF wave heating as shown in Fig. 10. The Cu line emission intensity and the radiation loss from the main plasma started to increase around t = 7.55 s. At the same time, the line-integrated divertor plasma density was sharply reduced at a time scale of ~10 ms as well as the Dα emission intensity from the divertor. These results support the above conclusion that the reduction of the divertor plasma density on a short time scale and a large reduction ratio could be ascribed to the change of plasma-wall interaction due mainly to a reduction of the heat flux to the divertor plate.

The recycling coefficient's dependence on the heat and particle fluxes is strongly affected by the wall condition. The scattering of the time scale for the divertor plasma density drop could be related to the wall condition. When the recycling coefficient strongly depends on the particle and heat fluxes, the sharp drop in the divertor plasma density could be observed on a short time scale. For weak dependence, a relatively gradual decrease in divertor plasma density could be obtained. When the recycling coefficient is changed, keeping the recycling flux constant, the sharp drop of the Dα emission intensity could not be observed as the transition free H-mode in JT-60U. As for the EDA H-mode in Alcator C-Mode, the H'-mode and the HRS H-mode plasma in JFT-2M, a high level of Dα emission intensity was observed, where a change of plasma-wall interaction might affect the Dα emission intensity.

6. Summary

The transient response of the divertor plasma during the transition to the ELM free H-mode was investigated based on measurements with high time resolution and time-dependent divertor simulations. The time scale for the reduction of divertor plasma density was in the range of a few ms to several tens of ms. Simulations using the 2-D fluid divertor code UEDGE indicated that the time scale for the reduction of divertor plasma density was strongly affected by the recycling coefficient's dependence on the heat and particle fluxes. These results indicate that the fast reduction of divertor plasma density and Dα emission intensity on a time scale of a few ms with a large reduction ratio could be ascribed to the change of plasma-wall interaction depending on the heat and particle flux to the divertor plates. The scattering of the time scale for the drop in divertor plasma density could be related to the wall condition. Dα/Hα emission intensity should be used for the index of the H-mode condition, taking into consideration the change of plasma-wall interaction.

Acknowledgement

The authors wish to thank Dr. G.D. Porter, Dr. T.D. Rognlien, and Dr. M.E. Rensink for use of the UEDGE code.

[1] F. Wagner *et al.*, Phys. Rev. Lett. **49**, 1408 (1982).
[2] M. Greenwald *et al.*, Nucl. Fusion **37**, 793 (1997).
[3] K. Shinohara *et al.*, J. Plasma Fusion Res. **74**, 607 (1998).
[4] K. Kamiya *et al.*, Nucl. Fusion **43**, 1214 (2003).
[5] M. Kikuchi *et al.*, *Proc. 20th EPS Conf.* (Lisboa, 1993) Vol.**17C**, Part I (European Physical Society, 1993) p.179.
[6] K.H. Burrell *et al.*, Plasma Phys. Control. Fusion **44**, A253 (2002).
[7] H. Takenaga *et al.*, Rev. Sci. Instrum. **69**, 3181 (1998).
[8] D.G. Nilson *et al.*, Fusion Eng. Des. **34-35**, 609 (1997).
[9] A. Kukushkin *et al.*, J. Nucl. Mater. **290**, 887 (2001).
[10] T.D. Rognlien *et al.*, Contrib. Plasma Phys. **34**, 362 (1994).
[11] K. Shimizu *et al.*, J. Nucl. Mater. **313-316**, 1277 (2003).
[12] G.D. Porter *et al.*, J. Nucl. Mater. **313-316**, 1085 (2003).
[13] M.E. Fenstermacher *et al.*, Nucl. Fusion **45**, 1493 (2005).
[14] H. Takenaga *et al.*, Nucl. Fusion **41**, 1777 (2001).
[15] J.W. Davis and A.A. Haasz, J. Nucl. Mater. **241-243**, 37 (1997).
[16] H. Takenaga *et al.*, JAERI-Reviw **2003-029**, 62 (2003).
[17] A.V. Chankin *et al.*, J. Nucl. Mater. **313-316**, 828 (2003).
[18] H. Takenaga *et al.*, Nucl. Fusion **46**, S39 (2006).
[19] G.D. Porter *et al.*, J. Nucl. Mater. **313-316**, 1085 (2003).
[20] J. Biersack, W. Eckstein, Appl. Phys. A **34**, 73 (1984).
[21] D.A. Alman and D.N. Ruzic, Phys. Scr. **T111** 145 (2004).
[22] H. Takenaga and the JT-60 team, Phys. Plasmas **8**, 2217 (2001).